Doppler Water-Track Aided Inertial Navigation for Autonomous Underwater Vehicles

Øyvind Hegrenæs* Einar Berglund**

*Kongsberg Maritime Subsea, AUV Department, NO-3191 Horten, Norway
*Department of Engineering Cybernetics,
Norwegian University of Science and Technology, NO-7491 Trondheim, Norway
**Norwegian Defence Research Establishment, NO-2027 Kjeller, Norway.

***Abstract*—Navigation of underwater vehicles has been and remains a substantial challenge to all underwater platforms. With the emergence of new applications and the growing acceptance of autonomous underwater vehicles (AUVs) in both military and civilian institutions, comes the need for enhanced accuracy and robustness, sustainability, and de-risking. This paper reports the development and experimental evaluation of a state-of-the-art inertial navigation system (INS) for underwater vehicles. The proposed system improves underwater navigation capabilities both for vehicles lacking conventional velocity measurements, and for systems where the need for autonomy, robustness and integrity is important, e.g. during sensor dropouts or failures, or in case of emergency navigation. Together with real-time sea current estimation, Doppler velocity log (DVL) water-track measurements are integrated in the navigation system to provide velocity aiding for the INS. Complementary aiding sources include ultra short base line (USBL) acoustic positioning and DVL with bottom-track. The performance is evaluated on data from a field-deployed AUV, demonstrating the effectiveness, robustness, and sustainability of the proposed navigation system.**

I. Introduction

Despite significant effort, precise navigation remains a substantial challenge to all underwater platforms [1]. The actual autonomy of the vehicles in existence today is also limited. Further advances in both areas will enable new operations which earlier have been considered impractical or infeasible. Examples of emerging applications include fully autonomous naval operations, polar deployments and under ice surveys, pipeline inspection, and oceanographic research and fishery.

Several topics must be addressed, including state estimation research, improved near-bottom navigation, environmental estimation (e.g. sea current), and navigation in the mid-water zone. The latter also applies to descents or ascents in deep waters (e.g. during GPS surfacing). Future research should also accommodate increased level of autonomy [2], including the use of redundant and complementary measurements, terrain and feature-based navigation, and goal driven mission management. Methodologies for sensor and navigation system fault detection and isolation should also be developed [3].

In this paper we report the development and experimental evaluation of a state-of-the-art Doppler velocity log (DVL) water-track aided inertial navigation system (INS). Together with real-time sea current estimation, the water-relative measurements from the DVL are integrated in the navigation system to provide velocity aiding for the INS. As illustrated, this is an effective approach toward the solution to several of the above mentioned research challenges. Additional aiding sources include ultra short base line (USBL) acoustic positioning, pressure readings, and DVL bottom-track (DVLBT) when feasible. The integration of complementary velocity measurements enhances the precision, and even more importantly, the robustness and sustainability of the navigation system. The specific forces and angular rates in the INS are measured by a navigation grade inertial measurement unit (IMU).

The performance of the developed navigation system is evaluated on raw sensor data collected by a HUGIN 1000 AUV. Several scenarios are examined, including removal or outages of USBL and DVLBT data. The presented results verify that it is possible to significantly improve the accuracy, robustness and sustainability of the integrated INS by utilizing the DVL water-track (DVLWT) functionality. Besides being used for navigation, a sea current estimate may be of interest for other applications as well, e.g. oceanography and marine research, and autonomous mission planning and decision making.

It should be mentioned that an alternative to utilizing DVLWT velocities for aiding the INS is to take advantage of the insight provided by a kinetic vehicle. This has recently been reported in [4], [5]. As for earlier work on DVLWT aided INS the literature is scarce. Some examples of intergraded black-box systems for AUV navigation include [6], [7]. In [8] the authors utilize a deterministic observer for merging USBL and DVLWT data of an ROV. Another example is an individual diver hand-held navigation console, as reported in [9].

For the remainder, DVLWT-INS is used for short when discussing DVL water-track aided INS without distinguishing on accompanying sensors. Additional notation is appended as needed and when discussing the integration of specific aiding sensors such as USBL, surface GPS and DVLBT. Pressure sensor data are always included and used for aiding. This paper is furthermore organized as follows. The remainder of this section reviews notation and various kinematic relationships. Section II describes the integrated INS. The experimental setup is described in Section III, followed by an experimental evaluation of the proposed navigation system in Section IV, where in particular, the performance of the navigation system with and without DVLWT aiding is discussed.

A. Preliminaries

1) Notation: The coordinate-free position vector from the origin of frame $\{a\}$ to the origin of frame $\{b\}$ is given as $\vec{p}_{ab}$. Similarly, the angular velocity of $\{b\}$ relative to $\{a\}$ is written as $\vec{\omega}_{ab}$. For the linear velocity, the notation $\vec{v}_{ab}$ is slightly ambiguous as it does not indicate how it is derived from $\vec{p}_{ab}$. In light of this obscurity, the coordinate-free velocity vector of $\{b\}$ relative to $\{a\}$ may be written as $\vec{v}_{\underline{a}b}$ or $\vec{v}_{a\underline{b}}$, where the underline indicates the reference of differentiation. This is in agreement with the notation for kinematics proposed in [10].

A coordinate-vector is written in boldface. The position vector from $\{a\}$ to $\{b\}$ is then given as $\boldsymbol{p}^a_{ab}$, where the added superscript states which frame the vector is decomposed in. Note that the time derivative of a coordinate-vector does not require any additional notation since the differentiation is done in the immediate reference frame. If a prior reference of differentiation needs to be specified, this is done using the underline notation. This is illustrated in (1), where $[\vec{v}]^b \equiv \boldsymbol{v}^b$

$$\dot{\boldsymbol{v}}^b_{\underline{a}b} = \frac{d}{dt}\boldsymbol{v}^b_{\underline{a}b} = \frac{d}{dt}\left[\vec{v}_{\underline{a}b}\right]^b = \frac{d}{dt}\left[\frac{^a d}{dt}\vec{p}_{ab}\right]^b. \tag{1}$$

Recall that for any vectors $\boldsymbol{k}^a, \boldsymbol{k}^b \in \mathbb{R}^3$, $\boldsymbol{k}^b = \boldsymbol{R}^b_a \boldsymbol{k}^a$, where $\boldsymbol{R}^b_a$ is the rotation matrix from $\{b\}$ to $\{a\}$. A matrix $\boldsymbol{R}$ is a valid rotation matrix if $\boldsymbol{R} \in SO(3)$, where

$$SO(3) = \left\{\boldsymbol{R} \in \mathbb{R}^{3\times 3} : \det(\boldsymbol{R}) = 1, \boldsymbol{R}^\top \boldsymbol{R} = \boldsymbol{R}\boldsymbol{R}^\top = \boldsymbol{I}\right\}. \tag{2}$$

All matrices, including the identity matrix $\boldsymbol{I}$, are written in bold caps. Another commonly applied set is defined as

$$so(3) = \left\{\boldsymbol{S} \in \mathbb{R}^{3\times 3} : \boldsymbol{S} = -\boldsymbol{S}^\top\right\}. \tag{3}$$

From (3), and for any vector $\boldsymbol{k} = [k_1, k_2, k_3]^\top$, the skew-symmetric matrix operator $\boldsymbol{S}(\cdot) : \mathbb{R}^3 \mapsto so(3)$ is given as

$$\boldsymbol{S}(\boldsymbol{k}) = \begin{bmatrix} 0 & -k_3 & k_2 \\ k_3 & 0 & -k_1 \\ -k_2 & k_1 & 0 \end{bmatrix}. \tag{4}$$

Note that for all $\boldsymbol{k}, \boldsymbol{j} \in \mathbb{R}^3$, it follows that $\boldsymbol{S}(\boldsymbol{k})\boldsymbol{j} \equiv \boldsymbol{k} \times \boldsymbol{j}$.

2) Kinematics: Let $\{m\}$ denote a local coordinate frame where the origin is fixed at the surface of the WGS-84 Earth ellipsoid, and the orientation is north-east-down (NED). Similarly, let $\{w\}$ denote a reference frame where the origin is fixed to, and translates with the water (due to sea current). The current is assumed irrotational throughout this paper, which implies that each infinitesimal fluid element has zero angular velocity (spin). The frame $\{w\}$ is consequently defined such that it does not rotate relative to $\{m\}$. The sea current in this work is described entirely by the translational motion of $\{w\}$ relative to $\{m\}$. Recall that it is possible for a fluid traveling along a straight line to have vorticity, and similarly, for a fluid moving in a circle (or which changes direction) to be irrotational. For navigation purposes and INS, two additional reference frames are often used. The Earth-centered Earth-fixed (ECEF) frame is denoted $\{e\}$. The second frame $\{l\}$ is a wander azimuth frame. It is similar to $\{m\}$, but its origin is always located directly above the vehicle at the surface of the Earth ellipsoid. It is furthermore defined such that it has zero angular velocity relative to the rotating Earth about its z-axis. A last frame $\{b\}$ is a body-fixed frame where the axes coincide with the principal axes of the vehicle, and the origin located at the vehicle center of buoyancy (CB). Finally note that a submerged object will not rotate as it translates in an irrotational fluid flow. The assumption of irrotational current consequently implies that $\vec{\omega}_{mb} = \vec{\omega}_{wb}$.

TABLE I: Nomenclature

Description	Variable	Entries*
Local NED vehicle position	$\boldsymbol{p}^m_{mb}$	(x, y, z)
Vehicle attitude (roll, pitch, yaw)	$\boldsymbol{\Theta}$	(ϕ, θ, ψ)
Vehicle angular velocity	$\boldsymbol{\omega}^b_{mb} = \boldsymbol{\omega}^b_{eb} = \boldsymbol{\omega}^b_{wb}$	(p, q, r)
Earth-relative linear velocity	$\boldsymbol{v}^b_{\underline{m}b} = \boldsymbol{v}^b_{\underline{e}b}$	(u, v, w)
Earth-relative linear velocity	$\boldsymbol{v}^l_{\underline{m}b} = \boldsymbol{v}^l_{\underline{e}b}$	(u^l, v^l, w^l)
Water-relative linear velocity	$\boldsymbol{v}^b_{\underline{w}b}$	(u_r, v_r, w_r)
Current velocity	$\boldsymbol{v}^b_{\underline{m}w} = \boldsymbol{v}^b_{\underline{e}w}$	(u_c, v_c, w_c)
Current velocity	$\boldsymbol{v}^l_{\underline{m}w} = \boldsymbol{v}^l_{\underline{e}w}$	(u^l_c, v^l_c, w^l_c)

* Based on SNAME [11] notation

Based on the notation and reference coordinate frames described above, a general expression of the vehicle position may be written in coordinate-free form as

$$\vec{p}_{mb} = \vec{p}_{mw} + \vec{p}_{wb}. \tag{5}$$

Written in terms of velocities, the time derivative of (5) yields

$$\vec{v}_{\underline{m}b} = \vec{v}_{\underline{m}w} + \vec{v}_{\underline{w}b}, \tag{6}$$

where it was utilized that $\vec{\omega}_{mw} = 0$ due to the assumption of irrotational current. This is equivalent to $\boldsymbol{R}^m_w$ being time-invariant. Decomposed in $\{b\}$, (6) gives the relationship

$$\boldsymbol{v}^b_{\underline{m}b} = \boldsymbol{R}^b_m \boldsymbol{v}^m_{\underline{m}w} + \boldsymbol{v}^b_{\underline{w}b}. \tag{7}$$

Following along the same lines as above, a second important velocity relationship is given as

$$\boldsymbol{v}^l_{\underline{e}b} = \boldsymbol{v}^l_{\underline{e}w} + \boldsymbol{R}^l_b \boldsymbol{v}^b_{\underline{w}b}. \tag{8}$$

Note that $\boldsymbol{v}^b_{\underline{m}b}$ equals $\boldsymbol{v}^b_{\underline{e}b}$ since $\{m\}$ is fixed relative to $\{e\}$.

II. Underwater Vehicle Inertial Navigation

Following a brief review on INS, this Section describes the development of a DVLWT-INS. A second velocity aid is also integrated in the system using DVLBT. As is illustrated in Section IV, the application of complementary velocity measurements enhances the precision, and even more importantly, the robustness and sustainability of the integrated navigation system. The usage of DVLWT significantly increases both the accuracy and feasible operating time span of systems not having DVLBT. In the case both sources are available, the integrated navigation system is found to be far more robust to DVLBT dropouts. The INS sensitivity to the position measurement update frequency is also reduced throughout.

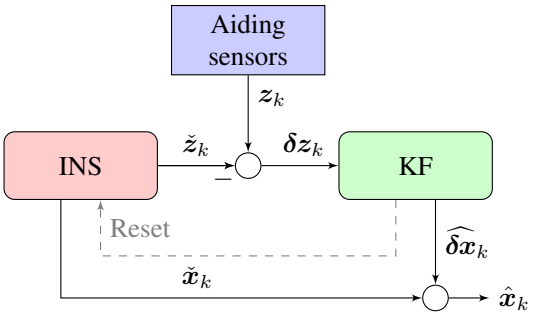

Fig. 1: Outline of conventional aided INS.

A. Brief review on INS

An INS calculates position, velocity and attitude using high frequency data from an IMU which typically consists of three accelerometers measuring specific force and three gyros measuring angular rate, all relative to the inertial space. Due to inherent errors in the gyros and accelerometers, the solution of the navigation equations embedded in the INS will have an unbounded drift unless counteracted. An aiding framework is consequently required to bind the error growth. An overview of INS aiding tools is given in [2], [12]. DVLWT aiding, as presented herein, is complementary to this set of tools.

In order to fuse the data from the INS and the aiding sensors some form of filtering must be implemented. This is typically accomplished using a Kalman filter (KF). An outline of a conventional aided INS is shown in Fig. 1, where the KF input is taken as the difference between the output from the appropriate aiding sensors and the INS. A perturbation method is used in this paper for deriving the INS error states. The states are included in the KF with the assumptions of small errors, i.e. first order approximation. The KF also estimates the colored errors of the different navigation sensors, as well as the sea current when utilizing DVLWT. The derivation of the KF measurement and process equations associated with the DVLBT, DVLWT, and the sea current are given subsequently. A schematic diagram of the integrated INS with complementary velocity aiding is shown in Fig. 2.

B. DVL Bottom-Track Aided INS

In many practical situations position measurements will be unavailable for extended periods of time and the INS will then chiefly depends on external velocity aiding. This is commonly archived using DVLBT which, if within sensor range, measures the vehicle linear velocity relative to the seabed along four acoustic beams. The information obtained from the pings in each beam is combined in order to calculate the velocity. Bottom-track from at least three beams is required.

The amount of literature on error sources and the use of DVLBT in underwater navigation is extensive. The reader is referred to [1], [12], [13]. Of underwater navigation systems incorporating DVLBT one may often distinguish between those based on INS, and those carrying out more traditional dead-reckoning by combining attitude information and DVLBT directly. Only the first case is considered in this work.

1) Measurement and Process Equations: The generalized vector of discrete inputs to the KF in Fig. 1 is given as

$$\boldsymbol{\delta z}_k \triangleq \boldsymbol{z}_k - \check{\boldsymbol{z}}_k, \tag{9}$$

where $\check{(\cdot)}$ denotes a calculated variable. For the linear velocity associated with the DVLBT we then get

$$\boldsymbol{\delta z}_{vel}^{\mathrm{DVLBT}} \triangleq \boldsymbol{z}_{vel}^{\mathrm{DVLBT}} - \check{\boldsymbol{z}}_{vel}^{\mathrm{INS}}, \tag{10}$$

where the sample index has been dropped for brevity. Substituting for the variables on the right hand side of (10) yields

$$\boldsymbol{\delta z}_{vel}^{\mathrm{DVLBT}} = \check{\boldsymbol{R}}_b^l \tilde{\boldsymbol{v}}_{\underline{e}b}^b - \check{\boldsymbol{v}}_{\underline{e}b}^l, \tag{11}$$

where $\tilde{(\cdot)}$ denotes a measured quantity. The variables $\check{\boldsymbol{v}}_{\underline{e}b}^l$ and $\check{\boldsymbol{R}}_b^l$ stem from the INS, and $\tilde{\boldsymbol{v}}_{\underline{e}b}^b$ is the Earth-relative velocity measured by the DVLBT. Note that any misalignment between the DVL instrument frame and the body frame, as well as scale effects due to erroneous speed of sound in the DVL, should be sought compensated for prior to applying $\tilde{\boldsymbol{v}}_{\underline{e}b}^b$ in the KF.

A calculated or measured variable may be considered as a sum of its true value and a corresponding error, that is,

$$\check{(\cdot)} = (\cdot) + \delta(\cdot) \quad \text{and} \quad \tilde{(\cdot)} = (\cdot) + \delta(\cdot). \tag{12}$$

Substituting with errors and true values in (11) yields

$$\boldsymbol{\delta z}_{vel}^{\mathrm{DVLBT}} = \boldsymbol{\delta R}_b^l \boldsymbol{R}_b^l (\boldsymbol{v}_{\underline{e}b}^b + \boldsymbol{\delta v}_{\underline{e}b}^b) - (\boldsymbol{v}_{\underline{e}b}^l + \boldsymbol{\delta v}_{\underline{e}b}^l), \tag{13}$$

where $\boldsymbol{\delta R}_b^l \in SO(3)$ is a measure of the deviation between the true rotation matrix and the rotation matrix calculated by the INS. For small errors it can be shown that $\boldsymbol{\delta R}_b^l \approx \boldsymbol{I} + \boldsymbol{S}(\boldsymbol{e}_{lb}^l)$, where $\boldsymbol{e}_{lb}^l$ is a vector of angle-axis errors [14]. Returning to (13), the final expression for the measurement equation associated with the DVLBT may be written to first order as

$$\boldsymbol{\delta z}_{vel}^{\mathrm{DVLBT}} = \boldsymbol{R}_b^l \boldsymbol{\delta v}_{\underline{e}b}^b - \boldsymbol{\delta v}_{\underline{e}b}^l - \boldsymbol{S}(\boldsymbol{v}_{\underline{e}b}^l)\boldsymbol{e}_{lb}^l. \tag{14}$$

Both $\boldsymbol{\delta v}_{\underline{e}b}^l$ and $\boldsymbol{e}_{lb}^l$ are included as states in the KF process equation. Note that (14) is not directly realizable since it depends on the true velocity and orientation, i.e. $\boldsymbol{v}_{\underline{e}b}^l$ and $\boldsymbol{R}_b^l$. When implementing the KF, the best a-priori estimates are used in lieu, calculated according to

$$\bar{\boldsymbol{v}}_{\underline{e}b}^l \triangleq \check{\boldsymbol{v}}_{\underline{e}b}^l - \bar{\boldsymbol{\delta v}}_{\underline{e}b}^l \quad \text{and} \quad \bar{\boldsymbol{R}}_b^l \triangleq [\boldsymbol{I} - \boldsymbol{S}(\bar{\boldsymbol{e}}_{lb}^l)]\check{\boldsymbol{R}}_b^l, \tag{15}$$

where $\bar{(\cdot)}$ denotes the most recent or best a-priori estimate prior to the KF measurement update or correction.

It is assumed in this work that the DVLBT output error $\boldsymbol{\delta v}_{\underline{e}b}^b$ can be modeled as the sum of colored noise and zero-mean white noise. The entries of $\boldsymbol{\delta v}_{\underline{e}b}^b$ are considered uncorrelated. If we let $\boldsymbol{\Delta v}$ and $\boldsymbol{\xi}$ denote the colored and white noises, respectively, the error can be expressed as

$$\boldsymbol{\delta v}_{\underline{e}b}^b = \boldsymbol{\Delta v}_{\underline{e}b}^b + \boldsymbol{\xi}_{v_{\underline{e}b}^b}. \tag{16}$$

While white noise is isolated in time, a colored process is local in time since its value at one instant also depends on prior values. Numerous correlation models can be used, depending on the presumed noise characteristics [15], [16]. The colored noise in (16) is embedded in the KF as a zero-mean first order Markov process driven by white noise, that is,

$$\dot{\boldsymbol{\Delta v}}_{\underline{e}b}^b = -\boldsymbol{T}_{\Delta v_{\underline{e}b}^b}^{-1} \boldsymbol{\Delta v}_{\underline{e}b}^b + \boldsymbol{\gamma}_{\Delta v_{\underline{e}b}^b}. \tag{17}$$

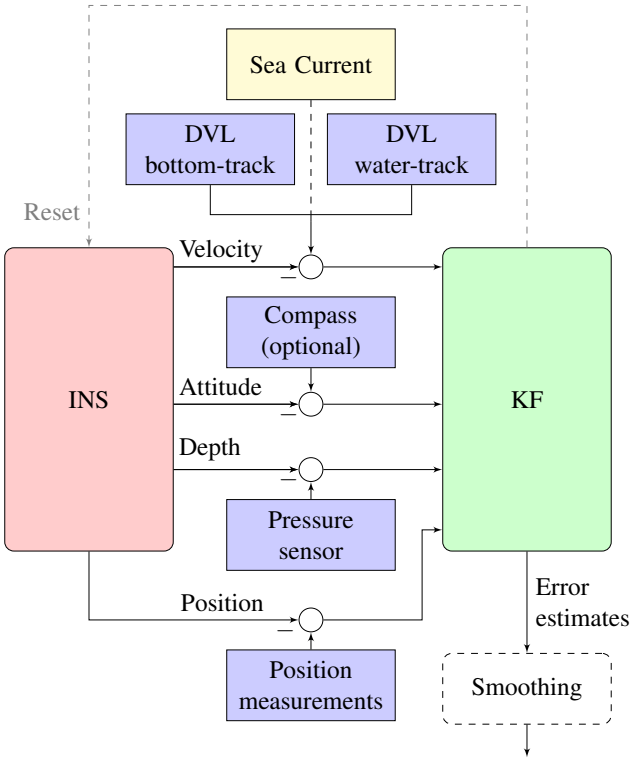

Fig. 2: Schematic diagram of the integrated INS with complementary velocity aiding. Various operational scenarios are investigated in this work, including removal or dropouts of DVLBT and position measurements. The latter may be available often or only sporadically.

C. DVL Water-Track Aided INS and Sea Current Estimation

Even when including DVLBT, situations may arise where it fails to work or measurements are discarded due to reduced quality. This will for instance occur when operating above the DVLBT sensor range, e.g. during GPS surfacing or long descents in deep waters, or regular operations in the mid-water zone. DVLBT may also be lost over rough bathymetry. In any case, in the absence of DVLBT, alternative velocity information is required to achieve an acceptable low drift INS solution between position updates. One possibility is to utilize DVLWT in conjunction with real-time sea current estimation. In general the current will constitute the dominant error source when utilizing DVLWT, hence it needs to be accounted for.

1) Measurement and Process Equations: Following along the same lines as in Section II-B, the error velocity related to the DVLWT is defined as

$$\boldsymbol{\delta z}_{vel}^{\mathrm{DVLWT}} \triangleq \boldsymbol{z}_{vel}^{\mathrm{DVLWT}} - \check{\boldsymbol{z}}_{vel}^{\mathrm{INS}}. \tag{18}$$

Furthermore, motivated by (8) the generalized linear velocity associated with the DVLWT and sea current is defined as

$$\boldsymbol{z}_{vel}^{\mathrm{DVLWT}} \triangleq \check{\boldsymbol{v}}_{\underline{e}w}^{l} + \check{\boldsymbol{R}}_{b}^{l}\tilde{\boldsymbol{v}}_{\underline{w}b}^{b}, \tag{19}$$

where $\tilde{\boldsymbol{v}}_{\underline{w}b}^{b}$ is the water-relative linear velocity measured by the DVLWT and $\tilde{\boldsymbol{v}}_{\underline{e}w}^{l}$ is the calculated sea current velocity. As earlier $\check{\boldsymbol{R}}_{b}^{l}$ stem from the INS. Substituting for the variables on the right hand side of (18) gives the expression

$$\boldsymbol{\delta z}_{vel}^{\mathrm{DVLWT}} = \check{\boldsymbol{v}}_{\underline{e}w}^{l} + \check{\boldsymbol{R}}_{b}^{l}\tilde{\boldsymbol{v}}_{\underline{w}b}^{b} - \check{\boldsymbol{v}}_{\underline{e}b}^{l}. \tag{20}$$

Note that if the sea current was measured it should be used in place of $\check{\boldsymbol{v}}_{\underline{e}w}^{l}$. In this paper we assume that $\check{\boldsymbol{v}}_{\underline{e}w}^{l} = \boldsymbol{0}$, which is to say that our best a-priori guess of the current is zero. It does not mean that the true current is zero. As shown subsequently, the true sea current is estimated in the navigation system KF.

Substituting with errors and true values in (20) yields

$$\begin{aligned}\boldsymbol{\delta z}_{vel}^{\mathrm{DVLWT}} = (\boldsymbol{v}_{\underline{e}w}^{l} + \boldsymbol{\delta v}_{\underline{e}w}^{l}) + \boldsymbol{\delta R}_{b}^{l}\boldsymbol{R}_{b}^{l}(\boldsymbol{v}_{\underline{w}b}^{b} + \boldsymbol{\delta v}_{\underline{w}b}^{b}) \\ - (\boldsymbol{v}_{\underline{e}b}^{l} + \boldsymbol{\delta v}_{\underline{e}b}^{l}),\end{aligned} \tag{21}$$

where $\boldsymbol{\delta R}_{b}^{l}$ is the attitude deviation matrix, as described above. From the relationship in (8) and under the assumption of small orientation errors, (21) can be written to first order as

$$\boldsymbol{\delta z}_{vel}^{\mathrm{DVLWT}} = \boldsymbol{\delta v}_{\underline{e}w}^{l} + \boldsymbol{R}_{b}^{l}\boldsymbol{\delta v}_{\underline{w}b}^{b} - \boldsymbol{\delta v}_{\underline{e}b}^{l} - \boldsymbol{S}(\boldsymbol{v}_{\underline{w}b}^{l})\boldsymbol{e}_{lb}^{l}. \tag{22}$$

The dependency to $\boldsymbol{v}_{\underline{w}b}^{l}$ can be removed by applying (8) a second time and by recognizing that $\boldsymbol{v}_{\underline{e}w}^{l} = -\boldsymbol{\delta v}_{\underline{e}w}^{l}$. The final expression for the measurement equation associated with the DVLWT and the sea current is given to first order as

$$\boldsymbol{\delta z}_{vel}^{\mathrm{DVLWT}} = \boldsymbol{\delta v}_{\underline{e}w}^{l} + \boldsymbol{R}_{b}^{l}\boldsymbol{\delta v}_{\underline{w}b}^{b} - \boldsymbol{\delta v}_{\underline{e}b}^{l} - \boldsymbol{S}(\boldsymbol{v}_{\underline{e}b}^{l})\boldsymbol{e}_{lb}^{l}. \tag{23}$$

The latter equation clearly resembles the expression in (14). As in the DVLBT case, the best a-priori estimates are used in place of $\boldsymbol{R}_{b}^{l}$ and $\boldsymbol{v}_{\underline{e}b}^{l}$, calculated according to (15).

It is assumed herein that both the DVLWT error $\boldsymbol{\delta v}_{\underline{w}b}^{b}$ and the a-priori current prediction error $\boldsymbol{\delta v}_{\underline{e}w}^{l}$ can be modeled as the sum of colored noise and zero-mean white noise. The entries of both $\boldsymbol{\delta v}_{\underline{w}b}^{b}$ and $\boldsymbol{\delta v}_{\underline{e}w}^{l}$ are considered uncorrelated. If we let $\boldsymbol{\Delta v}$ and $\boldsymbol{\xi}$ denote the colored and white noises, respectively, the errors can be expressed as

$$\boldsymbol{\delta v}_{\underline{w}b}^{b} = \boldsymbol{\Delta v}_{\underline{w}b}^{b} + \boldsymbol{\xi}_{v_{\underline{w}b}^{b}} \tag{24}$$

$$\boldsymbol{\delta v}_{\underline{e}w}^{l} = \boldsymbol{\Delta v}_{\underline{e}w}^{l} + \boldsymbol{\xi}_{v_{\underline{e}w}^{l}}. \tag{25}$$

The colored noises in (24)-(25) are implemented as zero-mean first order Markov processes driven by white noise, that is,

$$\dot{\boldsymbol{\Delta v}}_{\underline{w}b}^{b} = -\boldsymbol{T}_{\Delta v_{\underline{w}b}^{b}}^{-1}\boldsymbol{\Delta v}_{\underline{w}b}^{b} + \boldsymbol{\gamma}_{\Delta v_{\underline{w}b}^{b}} \tag{26}$$

$$\dot{\boldsymbol{\Delta v}}_{\underline{e}w}^{l} = -\boldsymbol{T}_{\Delta v_{\underline{e}w}^{l}}^{-1}\boldsymbol{\Delta v}_{\underline{e}w}^{l} + \boldsymbol{\gamma}_{\Delta v_{\underline{e}w}^{l}}. \tag{27}$$

The colored noises are states in the KF process equation. Recall that the estimate of $\boldsymbol{\Delta v}_{\underline{e}w}^{l}$ is also an estimate of $\boldsymbol{\delta v}_{\underline{e}w}^{l}$. Negated, this is again an estimate of the true sea current.

III. Experimental Setup

An overview of the experimental setup, including vehicle particulars, employed navigation sensors, mission trajectories, and the processing of raw navigation data, is given in this section. The experimental results are discussed in Section IV.

Fig. 3: HUGIN 1000 onboard H.U. Sverdrup II

TABLE II: IMU specifications

	Bias		Scale Factor		
Model	Gyro	Acc	Gyro	Acc	**Rate**
Honeywell HG9900	0.003 deg/h	25 μg	5 PPM	100 PPM	300 Hz

TABLE III: Primary navigation aiding sensors

Variable	**Sensor**	**Precision**	**Rate**
Position	Kongsberg HiPAP USBL* NovAtel GPS (onboard AUV)	$<$20 cm, 0.12 deg 1.8 m RMS	Varying** 1 Hz
Velocity	RDI DVL 300kHz RDI DVL 300kHz water reference	$\pm$0.4 %$\pm$0.2 cm/s	$>$1 Hz $>$1 Hz
Pressure	Paroscientific	0.01 % full scale	1 Hz

* Surface ship GPS and USBL are combined to give a global vehicle position. The accuracy of the final position also depends on the ship GPS precision.
** Stored topside at approximately 1/3 Hz. While submerged, the AUV receives position updates at about 1/30 Hz, from the surface via an acoustic link.

A. Vehicle Description

The performance and comparison of the integrated INS with and without DVLWT aiding is evaluated on raw sensor data collected by a HUGIN 1000 AUV with 3000 m depth rating. The vehicle is owned and operated by the Norwegian Defence Research Establishment (FFI). The launch and recovery system and the AUV are shown in Fig. 3. The diameter and length (base version) of the vehicle are 0.75 and 5.3 m. It can operate with full payload for 25 h at a cruising speed of about 2 m/s.

HUGIN 1000 is equipped with an aided INS, as outlined in Fig. 2. Some IMU specifications are shown in Table II. The primary navigation aiding sensors relevant to the data utilized in this work are listed in Table III. Additional aiding tools are also available but are not discussed any further in this paper.

B. Experiment Description

The data utilized in this paper were collected in the vicinity of 59° 29' N, 10° 28' E, in the Oslo-fjord, Norway. In the first part of the data the vehicle follows a straight line approximately 7 km in length, equivalent to about 1 h at nominal speed. The depth varies from 145 to 155 m. Note that navigating along a single straight line is considered worst case since there are no canceling effects, e.g. as seen when running a typical survey lawn-mover pattern [12]. In the second part the vehicle receives GPS measurements at the surface for a short period of time before descending to 165 m depth, where DVLBT measurements become available. The effect of including DVLWT aiding is investigated for both data sets.

C. Data Post-Processing

Raw navigation sensor values (without any filtering) are used throughout this paper. The HUGIN 1000 navigation system then re-processed the appropriate sensor data to get real-time estimates from the KF (this is done using a duplication of the vehicle at-sea navigation system). The re-navigation routines are implemented in NavLab [17], a tool which has been used extensively with all the HUGIN AUVs since the late 1990's. In addition to re-navigating the real-time navigation system, NavLab also contains offline smoothing functionality, based on a Rauch-Tung-Striebel (RTS) implementation. The RTS smoother utilizes both past and future sensor measurements and KF covariances, hence efficiently improving the integrity and accuracy of the final navigation solution [18]. In this paper the smoothed USBL-DVLBT-INS solution with the highest navigation sensor update rates available serves as the basis or reference when evaluating the performance of the DVLWT-INS and the different scenarios reported in this work. The accuracy of the RTS smoothed basis position was estimated to be 0.65 m (1σ) in north and east.

IV. Experimental Results

This section evaluates the performance of the DVLWT-INS described in Section II. Unless mentioned otherwise, the USBL measurements are received regularly at about 1/3 Hz, and when applicable, the DVLBT, DVLWT and surface GPS measurements are processed at about 1 Hz. As mentioned in Section III-C, the RTS smoothed basis solution serves as the ground truth during comparison. Unless stated otherwise, the evaluation of the navigation system and scenario in discussion is based on the real-time KF solution and its predicted estimation uncertainties. An estimation error is taken as the difference between the RTS basis solution and the solution from the integrated navigation system being evaluated.

A. Sparse or Reduced Frequency Position Updates

This experiment was done in order to evaluate the performance of the integrated INS in cases where position measurements are sparse or for some reason become unavailable for extended periods of time. This is a typical scenario for fully autonomous or covert operations in unknown areas, and in both civilian and military applications. Also, when covering large areas the vehicle may temporarily operate outside the range of the acoustics positioning, either this is facilitated by a surface ship, from an LBL grid, or from one or several UTP transponders [12]. While the solution for most AUVs to date is to utilize DVLBT to reduce the position error drift, this may not always be feasible as discussed in Section II-C.

The scenarios investigated in this section are best described from Fig. 4, where the navigation system receives position measurements at about 1/3 Hz for roughly 30 min. The measurements are then decimated or completely removed for the

TABLE IV: Sensor availability between 30 and 60 min

	Time between updates		
Experiment	USBL	DVLBT	DVLWT
Case 1.x	30 s		
Case 2.x	60 s		
Case 3.x	180 s	∅ s if x = 1,2	∅ s if x = 1,3
Case 4.x	300 s	0.7 s if x = 3,4	0.7 s if x = 2,4
Case 5.x	600 s		
Case 6.x	900 s		
Case 7.x	∅ s		

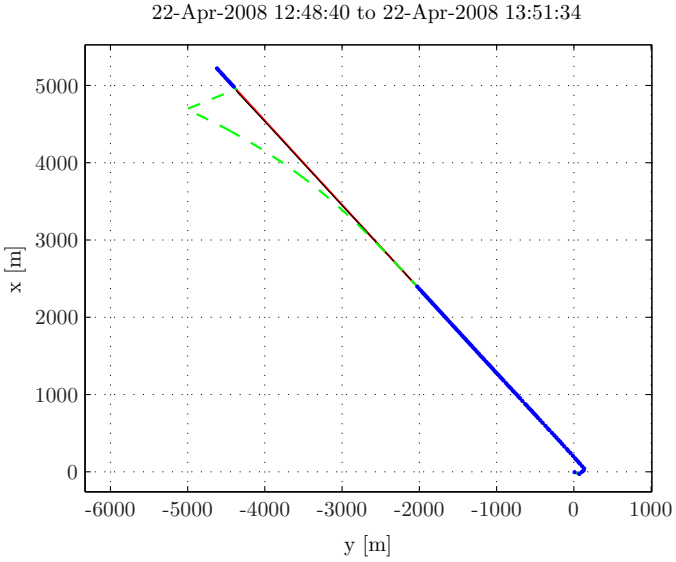

Fig. 4: The red (solid) trajectory is the horizontal basis position, with its initial location at the origin. The blue (•) data show the position measurements logged at about 1/3 Hz, according to Case 7 in Table IV. The segment without position aiding take place between 30 and 60 min. The black (solid) line is the real-time solution of the USBL-DVLWT-INS according to Case 7.2, and the green (dashed) is the corresponding solution of the regular USBL-INS.

next 30 min. The latter example is shown in Fig. 4. The sensor availability in the time period from 30 to 60 min is summarized in Table IV. When not available in this period, DVLBT or DVLWT measurements are not available exclusively.

As can be seen from Fig. 4, the navigation performance of the USBL-INS is clearly unsatisfactory when operating without position aiding for 30 min. Contrary, the USBL-DVLWT-INS performance remains good, as is illustrated in Fig. 5 and 6 for Case 7.2 and 6.2. In the first case the real-time horizontal position error is confined within 20 m. The precision may be further enhanced by doing smoothing, in which case the maximum error reduces to 6.5 m. The maximum real-time error of the USBL-INS is in the order of 700 m. A further comparison on the real-time performance is shown in Fig. 7a. The values are for the interval between 30 and 60 min. As anticipated, the significance of incorporating DVLWT in the navigation system becomes increasingly apparent as the position update frequency decreases. While the conventional USBL-INS is sensitive to the position update rate, the USBL-DVLWT-INS is considerably more robust and is able to keep

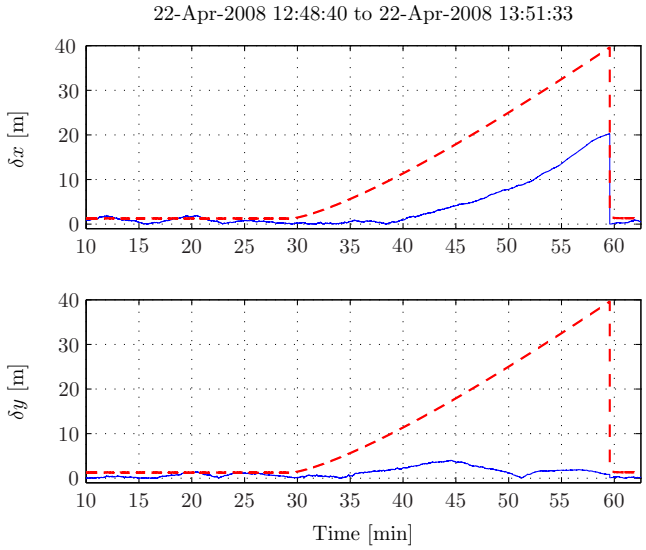

Fig. 5: The blue (solid) data show the absolute value of the north and east position errors for the USBL-DVLWT-INS, according to Case 7.2. The KF real-time uncertainties (1σ) are shown in red (dashed).

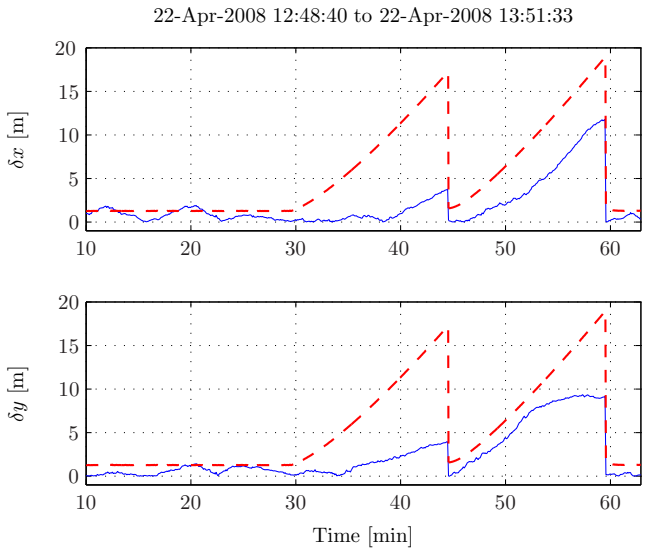

Fig. 6: Similar labels as in Fig. 5 but for Case 6.2.

the sustainability and accuracy of the navigation system at a satisfactory level even during long time periods without position updates. The different scenarios and results for the USBL-DVLWT-INS are summarized in Fig. 7b.

Another interesting and relevant question is whether the incorporation of DVLWT in the navigation system further enhances the precision obtained by the already accurate USBL-DVLBT-INS. As can be seen from Fig. 8, the performance of the USBL-DVLBT-DVLWT-INS is comparable or better than the USBL-DVLBT-INS throughout. While the impact is less striking than in the navigation system not having DVLBT, the improvement is clearly visible. As discussed earlier, and perhaps more importantly than the slight accuracy gain, is the significant robustness and sustainability improvement provided by the DVLWT-INS. This is discussed subsequently.

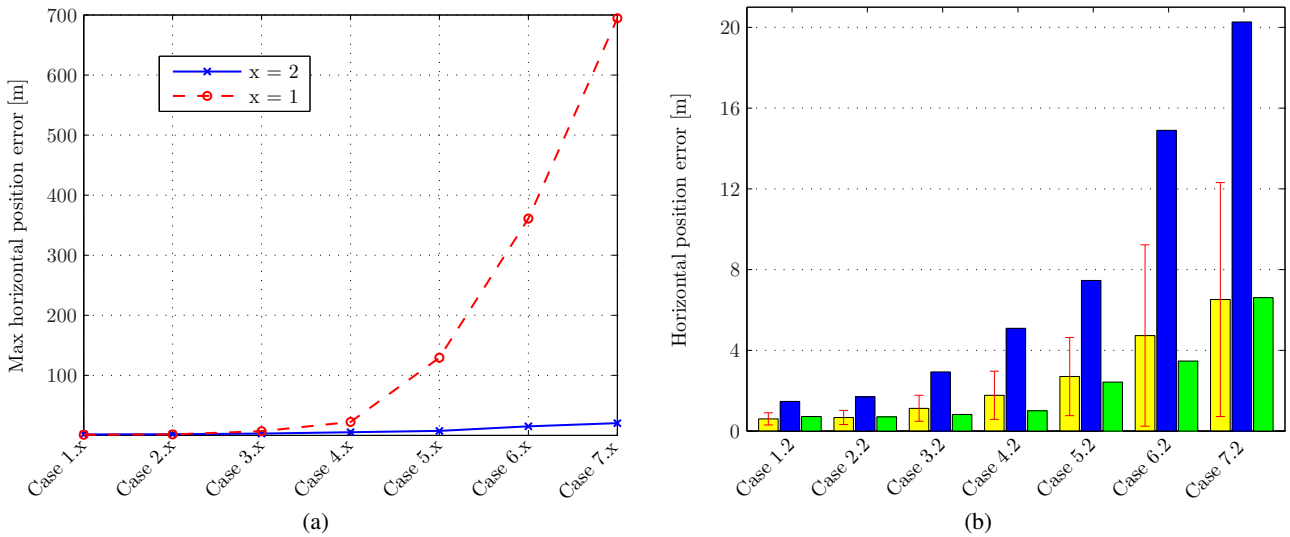

Fig. 7: Horizontal position estimation errors for Case .1 and .2 in Table IV: (a) Maximum horizontal position error with and without DVLWT aiding included. (b) The error bars from left to right show the mean and standard deviation of the real-time USBL-DVLWT-INS position error, the maximum real-time USBL-DVLWT-INS position error, and the maximum RTS smoothed USBL-DVLWT-INS position error.

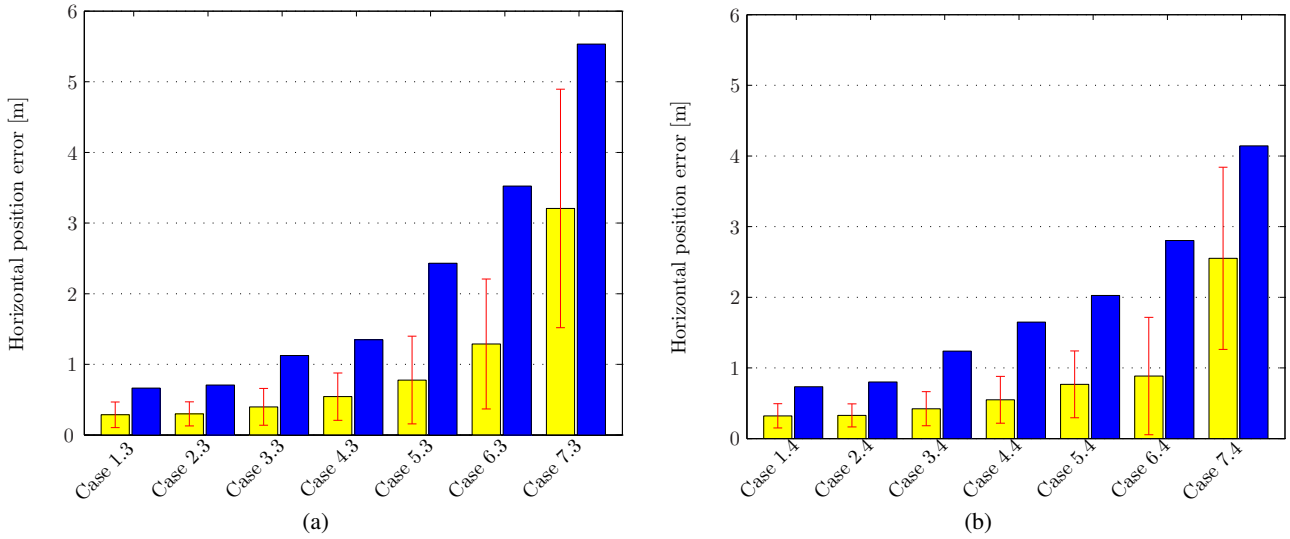

Fig. 8: Horizontal position estimation errors for Case 3 and 4 in Table IV: (a) The error bars from left to right show the mean and standard deviation of the real-time USBL-DVLBT-INS position error, and the maximum real-time USBL-DVLBT-INS position error. (b) Similar data and labels as in (a) but for the USBL-DVLBT-DVLWT-INS. The performance of the latter navigation system is slightly better.

B. DVL bottom-track dropouts

This experiment was done in order to evaluate the performance of the integrated INS in cases where DVLBT is included in the navigation sensor suite, but where measurements become unavailable. This will for instance occur when (possibly temporarily) operating above the sensor range or over rough bathymetry due to track-loss. Combined with few or no position measurements, the outcome may be damaging, and unacceptable for most autonomous or covert operations.

In the considered scenario the navigation system receives position measurements the first 5 min before becoming unavailable for the next 58 min, as shown in Fig. 9. During this time slot two DVLBT outages occur at 25 and 50 min, each lasting 10 min. For the data considered in this paper, and without these outages, the maximum error of the DVLBT-INS is about 11 m. In-situ navigation accuracy as low as 5 m (<0.1%) has been proven for the HUGIN 1000 when traveling along a straight line, as shown in Fig. 10. Perhaps more than the focus on better accuracy in systems with DVLBT (as shown) is the need for enhanced de-risking and robustness.

As can can be seen from Fig. 11 and 12, the navigation performance of the DVLBT-DVLWT-INS is significantly better than what is obtained with the DVLBT-INS. While the latter navigation system is vulnerable to the outages, the DVLWT-INS is more sustainable and is able to retain the accuracy at

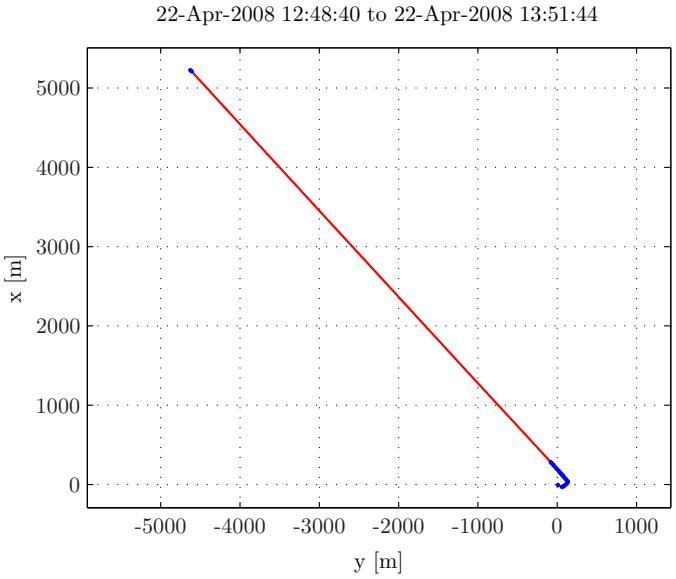

Fig. 9: The red (solid) trajectory is the horizontal basis position, with its initial location at the origin. The blue (•) data show the position measurements logged at about 1/3 Hz. The segment without position aiding take place between 5 and 63 min.

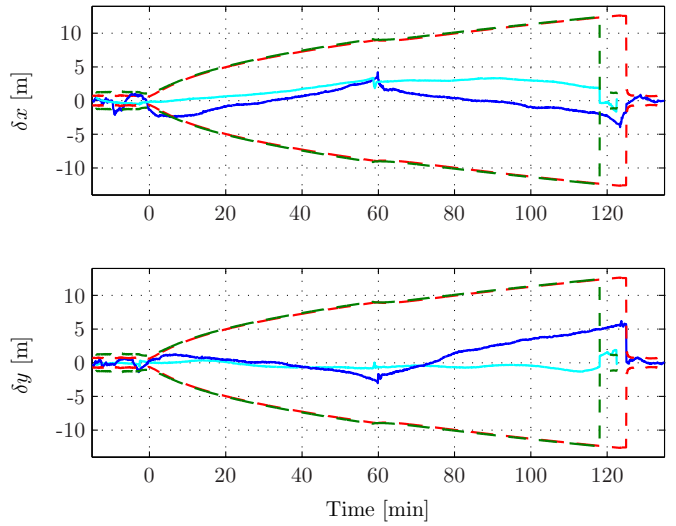

Fig. 10: Proven in-situ navigation performance of DVLBT-INS on HUGIN 1000 AUVs. The blue and cyan (solid) data show the north and east position errors. The KF real-time uncertainties (1σ) are shown in red and green (dashed). The trajectories were identical to the one shown in Fig. 9, but with one additional line, parallel and in opposite direction. The positioning aiding was turned off at time 0 and remained off for about 2 h (logging topside continued at 1/3 Hz).

a high level throughout. The maximum position errors of the DVLBT-DVLWT-INS with and without DVLBT outages are 9.5 m and 8.5 m, respectively. The corresponding maximum errors of the DVLBT-INS are 37 m and 11 m. Note that the precision of the DVLWT-INS depends on the accuracy of the estimated sea current. If consistent, and if the sea current does not change significantly during time slots without DVLBT (or USBL), the navigation accuracy will remain good.

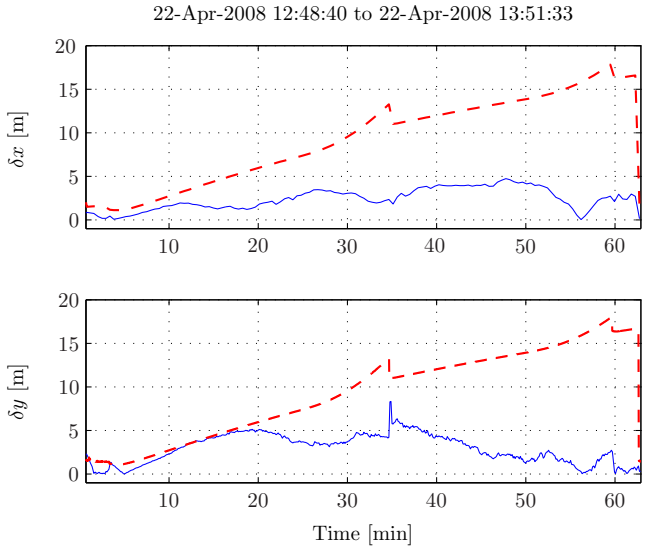

Fig. 11: The blue (solid) data show the absolute value of the north and east position errors for the DVLBT-DVLWT-INS when running without position aiding and where DVLBT is lost twice, 10 min each time. The KF real-time uncertainties (1σ) are shown in red (dashed).

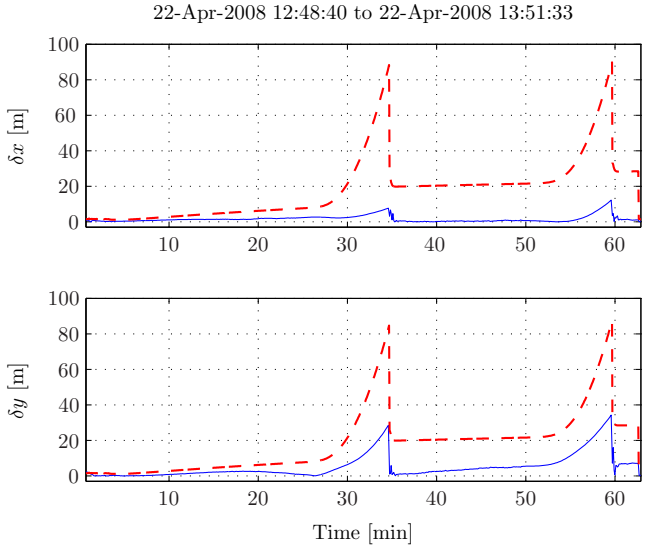

Fig. 12: Similar labels and data as in Fig. 11, but for the DVLBT-INS.

C. Sea Current Estimation

The ability to estimate sea current is of great importance when utilizing a navigation sensor that measures the vehicle velocity relative to the water. Any bias in the estimated sea current yields, if Earth-relative measurements (e.g. DVLBT and USBL) are absent, a direct position error drift in north and east. Besides being used for navigation, a sea current estimate may be of interest for other applications as well.

The estimated current of the DVLBT-DVLWT-INS (without outage) in Section IV-B is shown in Fig. 13, clearly filtered and more usable compared to that obtained by direct calculation. As furthermore shown in Fig. 14, the current is more observable when including DVLBT than USBL only, which

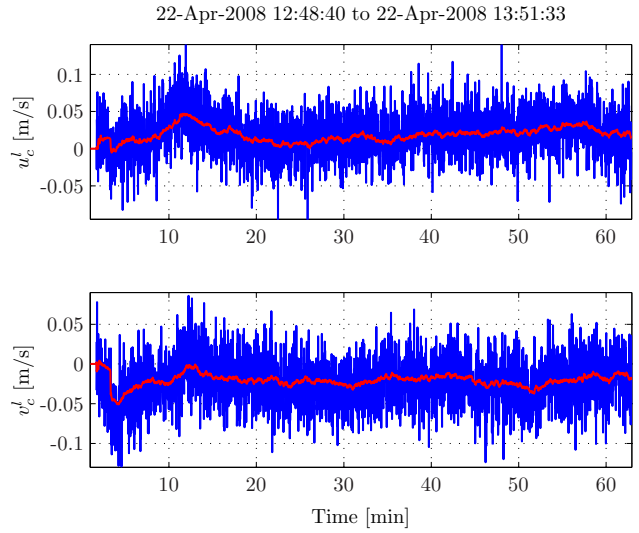

Fig. 13: Sea current in north and east. The blue data show the current calculated by directly applying (8) to raw DVLBT and DVLWT data, and by using the basis RTS smoothed attitude data. The red data show the real-time current estimates of the DVLBT-DVLWT-INS.

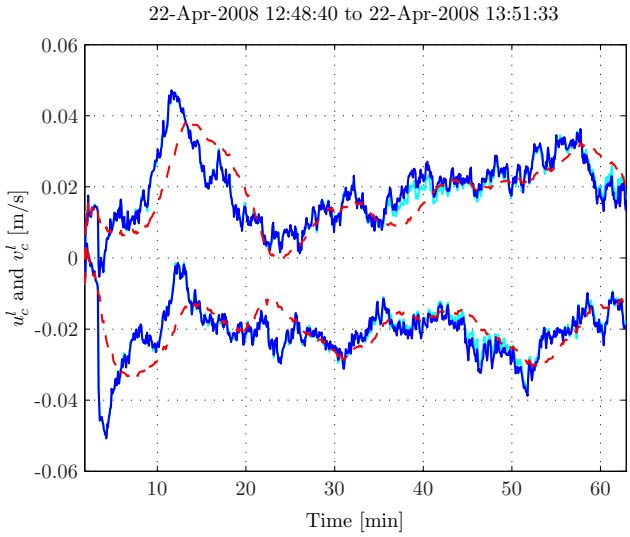

Fig. 14: Difference in real-time current estimates. The blue and cyan (solid) are both obtained from USBL-DVLBT-DVLWT-INS but the blue runs without USBL from 30 to 60 min, according to Case 7.4 in Table IV. The red (dashed) estimates are for the USBL-DVLWT-INS.

still yields a good estimate. The difference is due to the significantly more accurate point to point velocity accuracy and higher update rate of the DVLBT. Note that much of the observed time-lag may be removed in post-processing, as shown in Fig. 15. The same plot shows the real-time current estimate according to Case 7.2 in Section IV-A, illustrating the importance of choosing a suitable sea current time constant in the KF. Tuning the KF may be challenging since the current is highly stochastic and will vary in both place and time. For instance, while deeply submerged in open waters a long time constant (correlated with the tide) may be feasible, while a shorter value may be more desirable near the surface. This discussion is not elaborated upon any further in this paper, but should be given closer attention.

D. Descent and Ascent

For some underwater vehicles the need for accurate navigation during ascent, and particularly descent, may be of importance. This is certainly the case when the only mean for position updates is surface GPS, and the required real-time precision is high. Much can be done in post-processing (e.g. using NavLab [17]), yet a large deviation from the mission plan in real-time may result in mission failure nevertheless.

The effect of including DVLWT in the navigation system is briefly discussed in this section. The case is best described in Fig. 16, where surface GPS is recieved for about 2.5 min and DVLBT is retained at about 12 min after descending from the surface down to 165 m depth. The north and east position errors of the GPS-DVLWT-INS are shown in Fig. 17, where the maximum error prior to receiving DVLBT is about 5 m. The corresponding error when not including DVLWT is close to 40 m. The real-time north, east and down velocity errors and uncertainties for the DVLWT-INS are shown in Fig. 18. The estimation errors are consistent with the KF uncertainties.

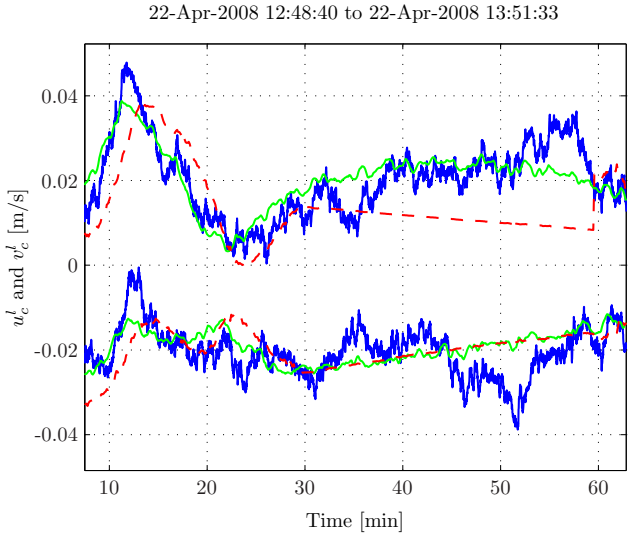

Fig. 15: Decay of current estimate when running without USBL and DVLBT. The blue (solid) are from the DVLBT-DVLWT-INS. The green (solid) and red (dashed) are the USBL-DVLWT-INS smoothed and real-time estimates, according to Case 7.2 in Table IV.

V. Conclusion

This paper has reported the development and experimental evaluation of a complete DVLWT-INS for underwater vehicle navigation. In combination with embedded sea current estimation, the use of DVLWT aiding is shown to be an effective approach toward the eventual solution of several emerging needs in underwater navigation, such as improved navigation in the mid-water zone, environmental estimation, and increased level of sustainability and robustness.

Various scenarios are considered, including sparse position updates, DVLBT outages, and navigation during descent. The inclusion of DVLWT in the navigation system is shown to significantly enhance the accuracy, and more importantly,

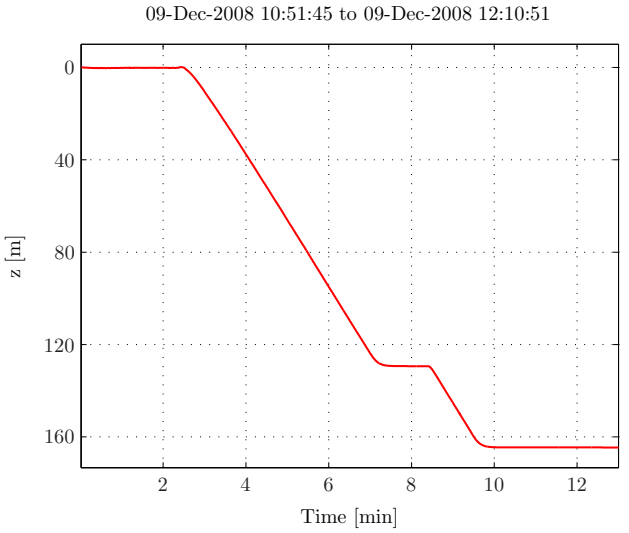

Fig. 16: Vehicle depth during descent from the surface down to 165 m.

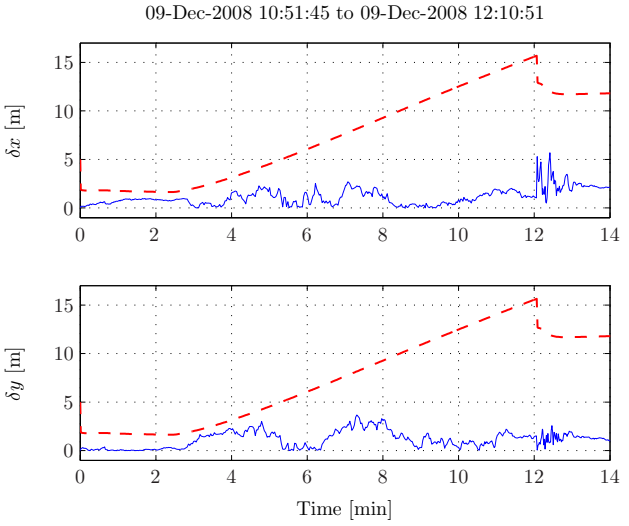

Fig. 17: The blue (solid) data show the absolute value of the north and east position errors for the GPS-DVLWT-INS during descent as shown on Fig. 16. The KF real-time uncertainties (1σ) are shown in red (dashed).

the robustness and sustainability of the integrated navigation system. The system is also shown to effectively estimate the sea current. Besides being used for navigation, a current estimate may be of interest for other applications as well, such as oceanography and marine research, and autonomous mission planning and decision making.

REFERENCES

[1] J. C. Kinsey, R. M. Eustice, and L. L. Whitcomb, "A survey of underwater vehicle navigation: Recent advances and new challenges," in *Proceedings of the 7th IFAC Conference of Manoeuvring and Control of Marine Craft*, Lisbon, Portugal, 2006.

[2] P. E. Hagen, Ø. Hegrenæs, B. Jalving, Ø. Midtgaard, M. Wiig, and O. K. Hagen, "Making AUVs truly autonomous," in *Underwater Vehicles*. Vienna: I-Tech Education and Publishing, January 2009.

[3] K. M. Fauske, O. Hallingstad, and Ø. Hegrenæs, "Toward a framework for high integrity navigation of autonomous underwater vehicles," in *Proceedings of the IFAC Workshop on Navigation, Guidance and Control of Underwater Vehicles*, Killaloe, Ireland, 2008.

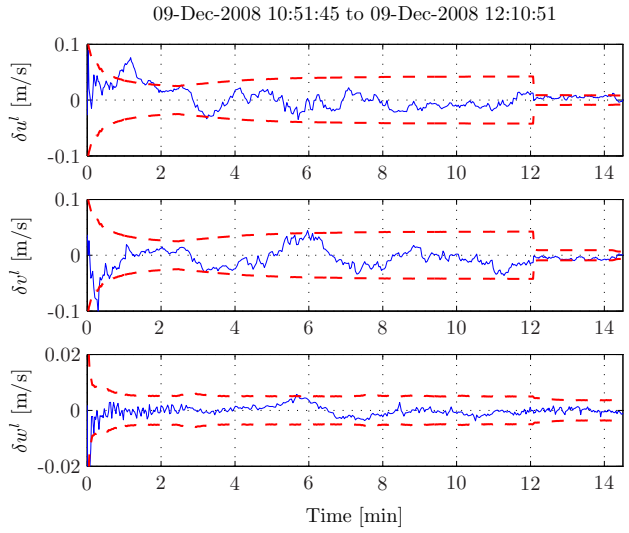

Fig. 18: North, east and down velocity errors and uncertainties. The blue (solid) data show the velocity errors for the GPS-DVLBT-DVLWT-INS, where DVLBT becomes available at 12 min. Similar data as in Fig. 17. The corresponding KF real-time uncertainties (1σ) are shown in red (dashed).

[4] Ø. Hegrenæs, E. Berglund, and O. Hallingstad, "Model-aided inertial navigation for underwater vehicles," in *Proceedings of the IEEE International Conference on Robotics and Automation*, Pasadena, CA, May 2008.

[5] Ø. Hegrenæs and O. Hallingstad, "Model-aided INS with sea current estimation for robust underwater navigation," *IEEE Journal of Oceanic Engineering*, Jan. 2009, submitted.

[6] S. Beiter, R. Poquette, B. S. Filipo, and W. Goetz, "Precision hybrid navigation system for varied marine applications," in *Proceedings of the IEEE Position Location and Navigation Symposium*, Palm Springs, CA, Apr. 1998.

[7] R. McEwen, H. Thomas, D. Weber, and F. Psota, "Performance of an AUV navigation system at arctic latitudes," *IEEE Journal of Oceanic Engineering*, vol. 30, no. 2, pp. 443–454, Apr. 2005.

[8] S. Augenstein and S. Rock, "Estimating inertial position and current in the midwater," in *Proceedings of the MTS/IEEE Oceans Conference and Exhibition*, Quebec, Canada, Sep. 2008.

[9] R. Hartman, W. Hawkinson, and K. Sweeney, "Tactical underwater navigation system (TUNS)," in *2008 IEEE/ION Position, Location and Navigation Symposium*, Monterey, CA, United states, 2008.

[10] K. Gade, "A unified notation for kinematics," In preparation.

[11] SNAME, "Nomenclature for treating the motion of a submerged body through a fluid," The Society of Naval Architects and Marine Engineers, Tech. Rep. Technical and Research Bulletin No. 1-5, 1950.

[12] B. Jalving, K. Gade, O. Hagen, and K. Vestgård, "A toolbox of aiding techniques for the HUGIN AUV integrated inertial navigation system," in *Proceedings of the MTS/IEEE Oceans Conference and Exhibition*, San Diego, CA, 2003.

[13] B. Jalving, K. Gade, K. Svartveit, A. Willumsen, and R. Sørhagen, "DVL velocity aiding in the HUGIN 1000 integrated inertial navigation system," *Modeling, Identification and Control*, vol. 25, no. 4, pp. 223–235, 2004.

[14] K. Gade, "Integrering av treghetsnavigasjon i en autonom undervanns-farkost (in Norwegian)," Norwegian Defence Research Establishment (FFI), Tech. Rep. FFI/RAPPORT-97/03179, 1997.

[15] A. Gelb, *Applied Optimal Estimation*. The MIT Press, 1974.

[16] X. R. Li and V. P. Jilkov, "Survey of maneuvering target tracking. Part I: Dynamic models," *IEEE Transactions on Aerospace and Electronic Systems*, vol. 39, no. 4, pp. 1333–1364, Oct. 2003.

[17] K. Gade, "NavLab, a generic simulation and post-processing tool for navigation," *European Journal of Navigation*, vol. 2, no. 4, pp. 21–59, Nov. 2004, (see also http://www.navlab.net/).

[18] A. B. Willumsen and Ø. Hegrenæs, "The joys of smoothing," in *Proceedings of the IEEE Oceans Conference and Exhibition*, Bremen, Germany, 2009.